THE JOURNAL OF PHYSICAL CHEMISTRY C
A JOURNAL OF THE AMERICAN CHEMICAL SOCIETY

pubs.acs.org/JPCC

Article

Surface-Enhanced Raman Spectroscopy on an As-deposited Fano Resonance Multilayer Substrate

Carmen Rizzuto, Antonio Ferraro,* Antonello Nucera, Giuseppe Emanuele Lio, Riccardo Cristoforo Barberi, and Marco Castriota*

Cite This: *J. Phys. Chem. C* 2023, 127, 12751−12759

Read Online

ACCESS | Metrics & More | Article Recommendations

ABSTRACT: In this work, we exploit the use of non-patterned multilayer thin films as substrates for surface-enhanced Raman spectroscopy (SERS) investigation. An appropriate selection of materials and thickness allows obtaining Fano resonance exhibiting high peak reflection at the same working wavelength of SERS apparatus. The proposed system is constituted by Ti/Ag/ZnO/Ag/Ti deposited on a glass substrate by a sputtering technique. The SERS effect provided by the Fano resonance was investigated by micro-Raman spectroscopy through the analysis of solutions of lithium perchlorate in propylene carbonate at salt concentrations of 0.1, 0.5, 1.0, and 2.0 M and compared to a reference substrate (glass substrate) with an average enhancement of all the bands around 3. The high flexibility in obtaining easily different resonance wavelengths combined with low cost and large area fabrication technology represents the main advantage of the proposed multilayer system for SERS investigation.

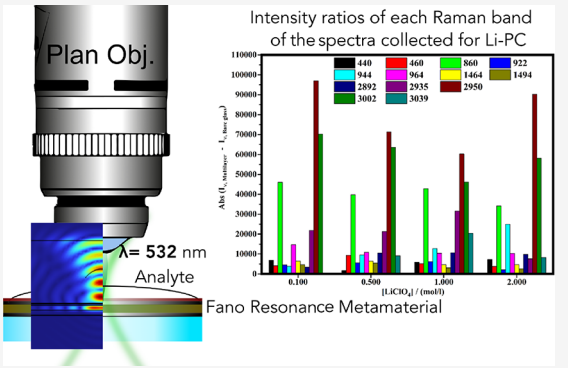

1. INTRODUCTION

Surface-enhanced Raman spectroscopy (SERS) is a non-destructive technique based on the improved Raman scattering of the molecules adsorbed on metallic surfaces.[1] SERS is a powerful and sensitive emission technique that was observed for the first time in 1973 on pyridine adsorbed on electrochemically roughened silver.[2] Two mechanisms were proposed for the observed enhancement: the first is the electromagnetic effect based on the excitation of localized surface plasmons,[3] while the second is explained by the chemical theory of the charge-transfer complex.[3] Substrates exhibiting SERS are commonly used for the identification of proteins,[4] biomolecules,[5] and chemical species including, for example, BTEX,[6] VOCs,[7] heavy metals,[8] pesticides,[9−11] and many others.[12−16]

The most common substrates for SERS are of three different classes: metal nanoparticles dispersed in colloidal suspensions, metal nanoparticles immobilized on solid substrates, and patterned nanostructures realized on a variety of substrates.[17,18] In all the above cases, a liquid analyte is in contact with a substrate enriched with metals such as gold, silver, and copper[3] for obtaining Vis-SERS and aluminum for UV-SERS.[19]

On the other hand, thin film multilayer systems can represent a very interesting alternative owing to their outstanding effects[20] such as electromagnetic mode confinement, plasmonic effect, self-collimation, and sharp resonances that found application in several fields as sensing,[21−23] structural color,[24,25] anticounterfeiting,[26−28] and cooling[29,30] to name a few.

In this work, we propose a novel approach for the easy and low-cost fabrication of a multilayer system exhibiting Fano resonance[31] usefully as a potential SERS substrate. The material and thickness configuration were selected to have a strong reflection peak at the working wavelength of the SERS apparatus (532 nm), leading to an enhancement of the electric field by a factor of more than five. Solutions of lithium perchlorate dissolved in propylene carbonate, at concentrations of 0.1, 0.5, 1, and 2 M, were investigated by micro-Raman spectroscopy for evaluating the SERS effect provided by the flat multilayer. The obtained results can be envisioned as a proof-of-concept work for the development of low-cost and disposable SERS substrates with advanced properties.

2. MATERIALS AND METHODS

Lithium perchlorate ($LiClO_4$), propylene carbonate (PC), acetone, and isopropyl alcohol were supplied by Sigma Aldrich Company.

Received: April 11, 2023
Revised: June 13, 2023
Published: June 23, 2023

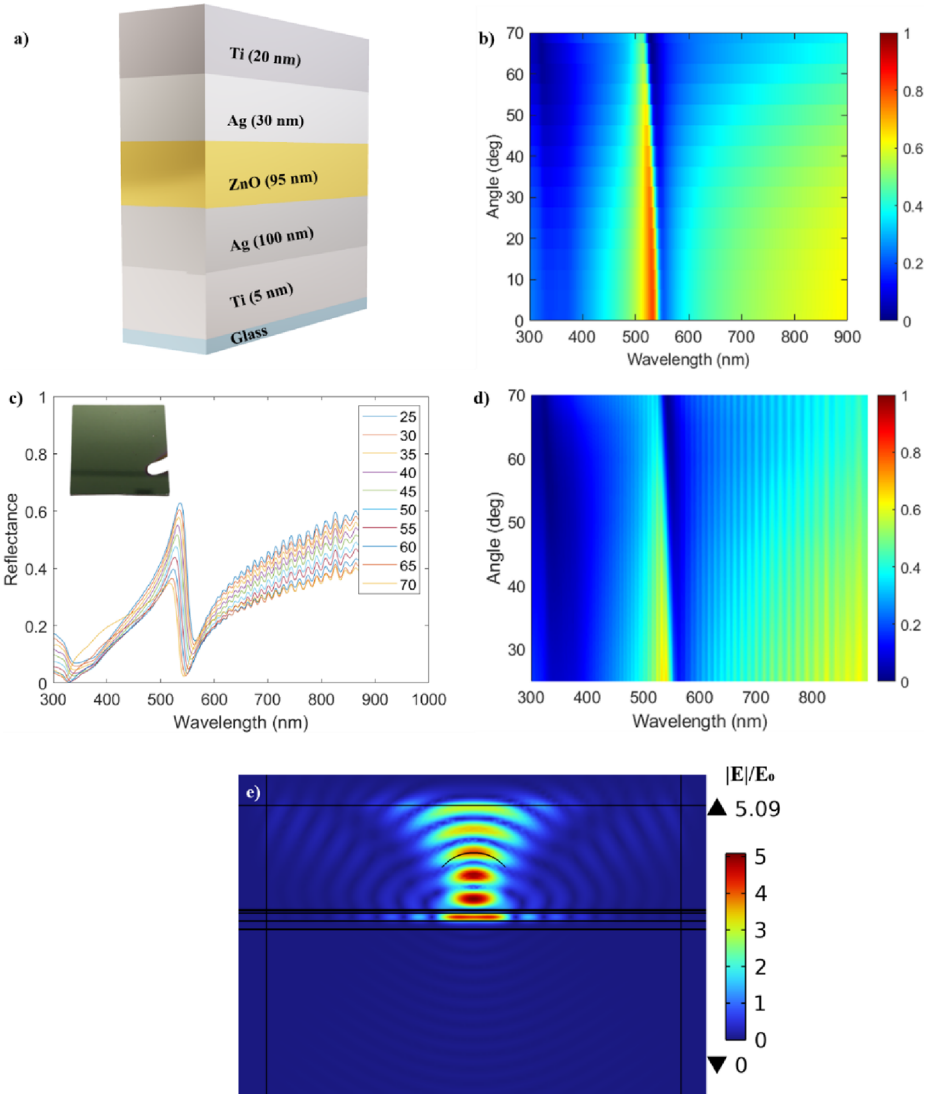

Figure 1. (a) Schematic representation of the multilayer system with thickness (horizontal lines) of the constituting layers. (b) Numerical reflectance maps varying the incident angle for the P-polarized electromagnetic wave. (c, d) Experimental reflected spectra and maps, respectively, varying the incident angle for the P-polarized electromagnetic wave for the proposed multilayer system shown in the inset. (e) Cross-sectional numerical electric field distribution map ($|E|/E_0$) at a wavelength of 532 nm.

2.1. Numerical Design of the Multilayer Substrate. The multilayer system was numerically designed using a transfer matrix method (TMM) implemented into MATLAB script. The final multilayer system is constituted of a glass support covered by an adhesive thin layer of 5 nm of titanium (Ti), then a 100 nm-thick reflective layer of silver (Ag), a 95 nm-thick cavity layer of zinc oxide (ZnO), another layer of Ag (30 nm), and, on the top, a 20 nm-thick layer of Ti. The electric field map was retrieved by using finite element method (FEM) implemented into COMSOL Multiphysics. For a better comparison with the experimental case, a modified input port resembling the microscope objective present in the setup was used for the simulation.

2.2. Fabrication and Characterization of the Multilayer Substrate. The proposed multilayer system was realized on microscope glass of dimension 2.5 cm × 2.5 cm. The glass substrate was cleaned with acetone and isopropyl alcohol and dried with nitrogen.

All the layers were deposited by sputtering technique using a Kenosistec-KS 053K20 machine with the following parameters: vacuum of 7×10^{-6} mbar, Ar pressure; Ti and Ag layers were deposited by using a DC cathode with a power of 100 W; a ZnO layer was deposited using an RF cathode with a power of 80 W. The times required for the sputtering are as follows: 90 s for Ti (5 nm), 207 s for Ag (100 nm), 1787 s for ZnO (95 nm), 62 s for Ag (30 nm), and 376 s for Ti (20 nm).

The fabricated systems were characterized at different incident angles using an ellipsometer (M-2000 by Woolam), working from 300 to 900 nm with a resolution of 1.5 nm.

2.3. Preparation of the Li-PC Solutions. Different solutions (Li-PC) composed of lithium perchlorate ($LiClO_4$) and propylene carbonate (PC) were prepared by dissolving, at room temperature, the salt in the solvent at the following concentrations: 0.1, 0.5, 1.0, and 2.0 M.

2.4. Micro-Raman Spectroscopy. Micro-Raman spectroscopy was performed using a Jobin Yvon micro-Raman LABRAM instrument equipped with a Nd:YAG laser (λ = 532 nm) as an excitation source with a maximum power of 50 mW. The spectrometer was equipped with a Peltier-cooled CCD

https://doi.org/10.1021/acs.jpcc.3c02406
J. Phys. Chem. C 2023, 127, 12751−12759

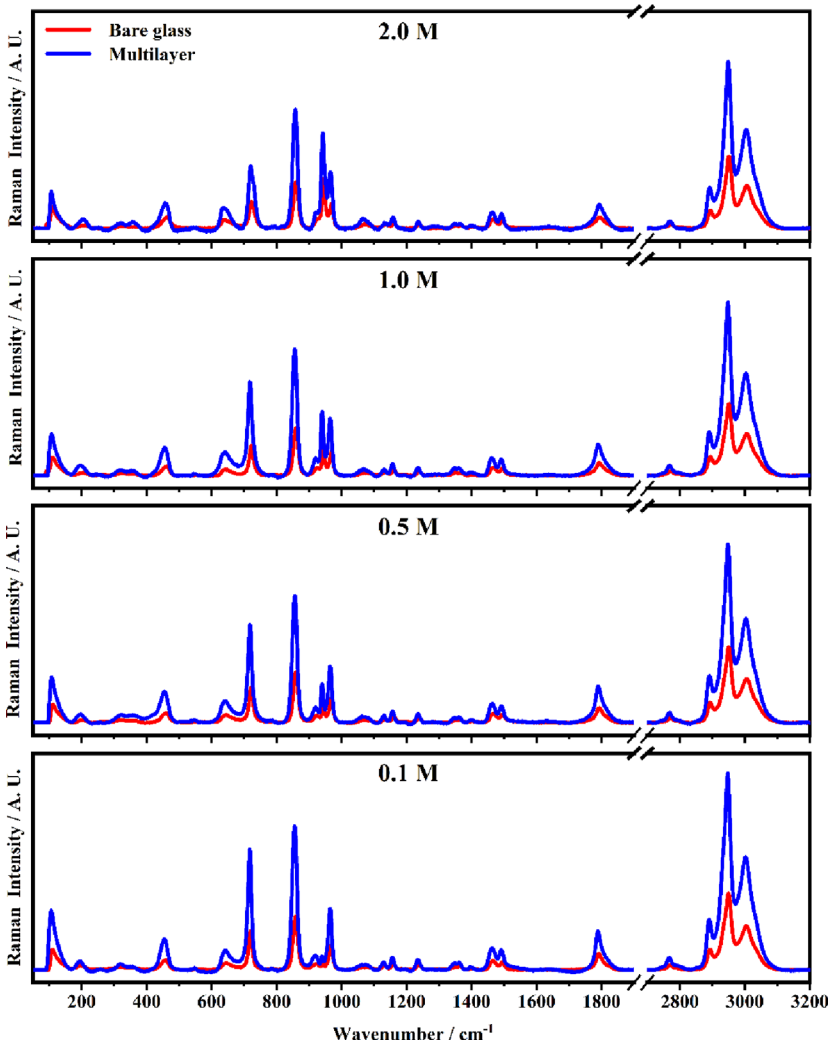

Figure 2. Representative Raman spectra, in the range between 50 and 3200 cm^{-1}, collected on lithium perchlorate and propylene carbonate (Li-PC) solutions at the concentrations 0.1, 0.5, 1.0, and 2.0 M deposited on the bare glass substrate (red lines) and multilayer substrate (blue lines). The break exists between 1900 and 2700 cm^{-1}, where there are no detectable Raman features.

detector at −70 °C. An Olympus 50× objective M-Plan NA = 0.50 was used to collect the Raman scattering signals.

3. RESULTS AND DISCUSSION

A schematic representation of the investigated multilayer system is reported in Figure 1a with the indication of each material thickness indicated as horizontal lines. The 5 nm Ti layer serves as adhesive with low influence on the resonance wavelength of the system. The following Ag-ZnO-Ag represents a narrowband absorber that is weakly coupled to the broadband absorber constituted by 30 nm of Ag and 20 nm of Ti, the latter having high loss in the visible range. This coupling produces an asymmetric Fano resonance, due to destructive interference,[31] with a high reflection peak at the resonance wavelength. The idea behind the proposed system is to maximize reflection at the working wavelength of the Raman apparatus and to exploit the confined reflected electric field for SERS investigation.

The proposed multilayer configuration exhibits a reflection peak at 532 nm with low angular dispersion, as presented in Figure 1b, which shows numerical reflectance by varying the incident angle for the P-polarized incident wave. The experimental reflectance, from 25 to 70°, agrees very well with the numerical one, as shown in Figure 1c,d, where a photograph of the fabricated multilayer is reported in the inset. Figure 1e reports the 2D cross-sectional numerical distribution map of the electric field amplitude, at the resonance wavelength, normalized to incident one (E_0), where $E_0 = \sqrt{\frac{P}{w}Z_0}$, here P is the input power, w represents the area illuminated by the light beam, and Z_0 is the impedance. The electric field is calculated using $|E|/E_0$, where $|E| = \sqrt[2]{E_x^2 + E_y^2 + E_z^2}$ of the proposed system. The map reveals a confinement inside the ZnO cavity but also an enhancement of more than 5 times on the top surface of the system, which strongly interacts with the sensing layer, leading to strengthening of Raman signals. The black arch line is the input port that resembles the experimental conditions. This input configuration is used to reproduce the numerical aperture of the objective and to focus the light on the surface on the proposed system.

To evaluate the SERS effect provided by the proposed multilayer system, a series of salt solutions of Li-PC at the following molar concentrations 0.1, 0.5, 1.0, and 2.0 M were investigated by micro-Raman spectroscopy on two different

https://doi.org/10.1021/acs.jpcc.3c02406
J. Phys. Chem. C 2023, 127, 12751−12759

substrates: a bare glass substrate, as reference, and glass covered with multilayer.

All the collected Raman spectra of the Li-PC solutions deposited on the multilayer substrate have higher intensity than those on the bare glass (see Figure 2). It means that the multilayer substrate behaves like a SERS surface due to the enhanced reflected electric field at the resonance wavelength.

The efficiency of the enhancement of the Raman scattering induced by the Fano multilayer system was studied by applying a deconvolution fitting procedure using the Voigt function on the bands observed in the ranges between 400 and 500 cm^{-1} (Figure 3), 800 and 1000 cm^{-1} (Figure 4), 1430 and 1550 cm^{-1} (Figure 5), and 2800 and 3200 cm^{-1} (Figure 6).

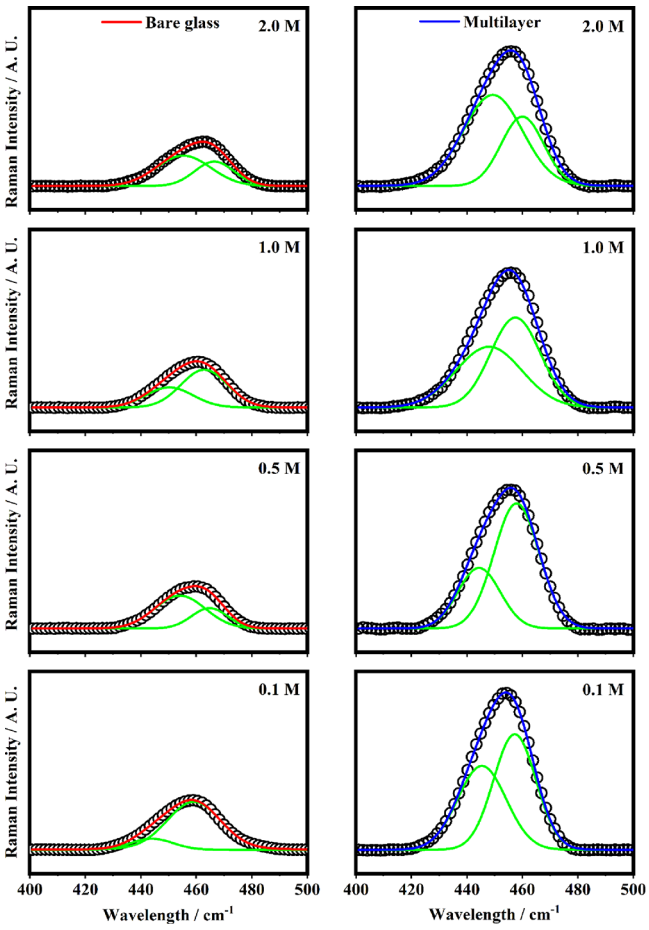

Figure 3. Fitting procedure of the Raman band in the range between 400 and 500 cm^{-1} collected on lithium perchlorate and propylene carbonate (Li-PC) solutions at the concentrations 0.1, 0.5, 1.0, and 2.0 M deposited on bare glass (on the left) and multilayer (on the right) substrates. The black circle represents the experimental data. The solid green lines are the Voigt curves, and the solid lines represent the total fit curves of the spectra collected on the bare glass (red) and multilayer (blue) substrates.

The Voigt profile is given by the combination of both Gaussian and Lorentzian functions.[32] In the range between 400 and 500 cm^{-1} (see Figure 3), the Raman band[33] at 455 cm^{-1} is due to the sum of two Voight curves assigned to a ClO_4^- anion scissoring mode (ν_2) and propylene carbonate deformation ring that fall at 440 and 460 cm^{-1}, respectively.

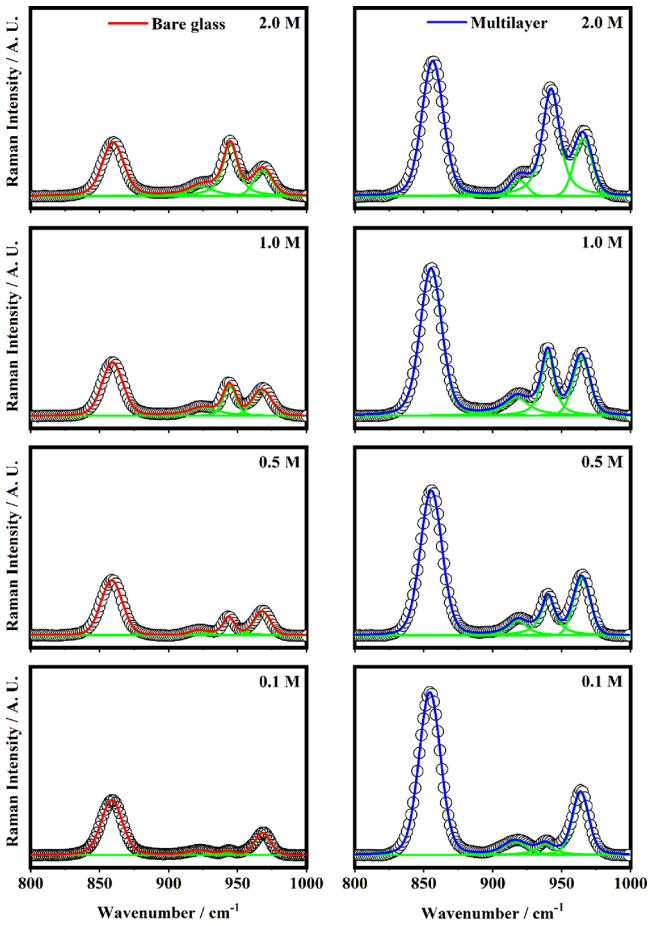

Figure 4. Fitting procedure of the Raman band in the range between 800 and 1000 cm^{-1} collected on lithium perchlorate and propylene carbonate (Li-PC) solutions at the concentrations 0.1, 0.5, 1.0, and 2.0 M deposited on bare glass (on the left) and multilayer (on the right) substrates. The black circle represents the experimental data. The solid green lines are the Voigt curves, and the solid lines represent the total fit curves of the spectra collected on the bare glass (red) and multilayer (blue) substrates.

Figure 4 shows the deconvolution band fitting in the range 800−1000 cm^{-1}, where four Voigt curves at 855, 922, 944, and 964 cm^{-1}, associated to specific modes, were used.

In fact, at 855 cm^{-1}, the strong band describing the symmetric ring deformation mode of the propylene carbonate is located.[33] The ν_1 free perchlorate mode was observed at 922 cm^{-1} in the tetrahedral geometry, and the variation of its band shape can be interpreted as an ion association in solutions.[34] The band at 944 cm^{-1} indicates the contact ion pair (Li^+-ClO_4^-) in propylene carbonate (PC), and its intensity increases when the $LiClO_4$ concentration increases.[33,35] The band at about 964 cm^{-1} is due to the symmetric stretching mode of the O-(C═O)-O group of the ring in the propylene carbonate.[36]

In Figure 5, the bands located in the range between 1430 and 1550 cm^{-1} are given by the superposition of two Voigt profiles centered at 1464 and 1494 cm^{-1}. The band at 1464 cm^{-1} is assigned to the asymmetric CH_3 deformation of propylene carbonate,[36] while the band at 1494 cm^{-1} is ascribed to the deformation mode of the O-CH_3 group of propylene carbonate.[36]

https://doi.org/10.1021/acs.jpcc.3c02406
J. Phys. Chem. C 2023, 127, 12751−12759

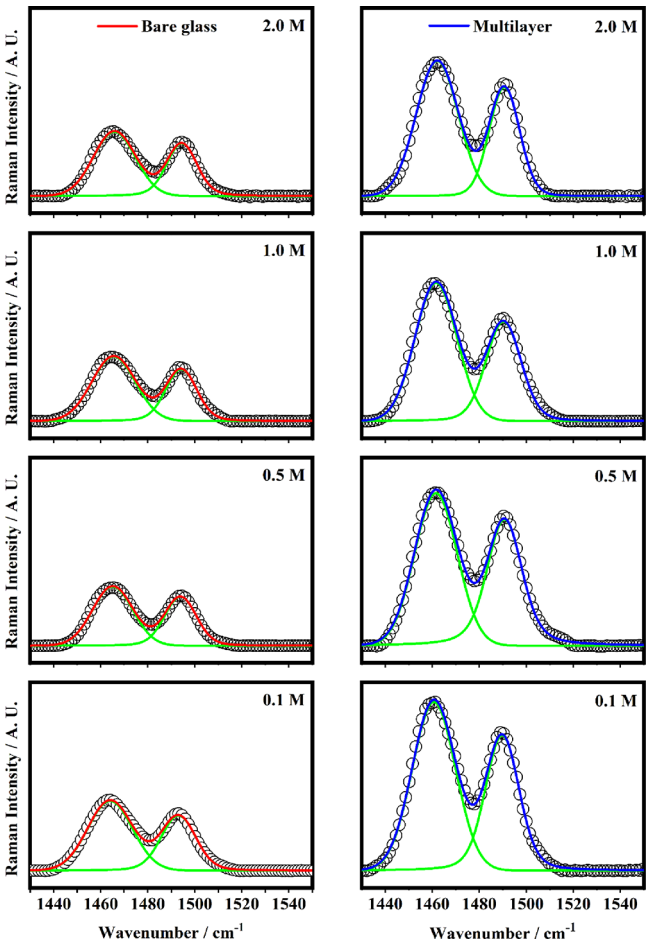

Figure 5. Fitting procedure of the Raman band in the range between 1430 and 1550 cm^{-1} collected on lithium perchlorate and propylene carbonate (Li-PC) solutions at the concentrations 0.1, 0.5, 1.0, and 2.0 M deposited on bare glass (on the left) and multilayer (on the right) substrates. The black circle represents the experimental data. The solid green lines are the Voigt curves, and the solid lines represent the total fit curves of the spectra collected on the bare glass (red) and multilayer (blue) substrates.

In the region between 2800 and 3200 cm^{-1}, the bands assigned to the C−H stretching modes of propylene carbonate were resolved into five components with the Voigt curves centered at 2892, 2935, 2950, 3002, and 3039 cm^{-1} (see Figure 6).

Using the proposed multilayer substrate, which exhibits Fano resonance and enhanced electric field, it is easy to generate a surface-enhanced Raman scattering signal. However, the accurate estimation of the enhancement factor (EF) shows some issues. The SERS signals are influenced by so many factors such as the Raman cross section of the molecules, the electrical field experienced by the molecules, and the number of molecules.[37]

To give a first quantitative evaluation of the SERS effect, the Raman intensities of the bands collected on the multilayer substrates were compared with the corresponding Raman intensities of the bands collected on bare glass, and the relative ratios defined in the eqs 1−4 are plotted in Figure 7 as a function of the concentration:

$$R_1 = \frac{I_{M,440} + I_{M,460}}{I_{G,440} + I_{G,460}} \quad (1)$$

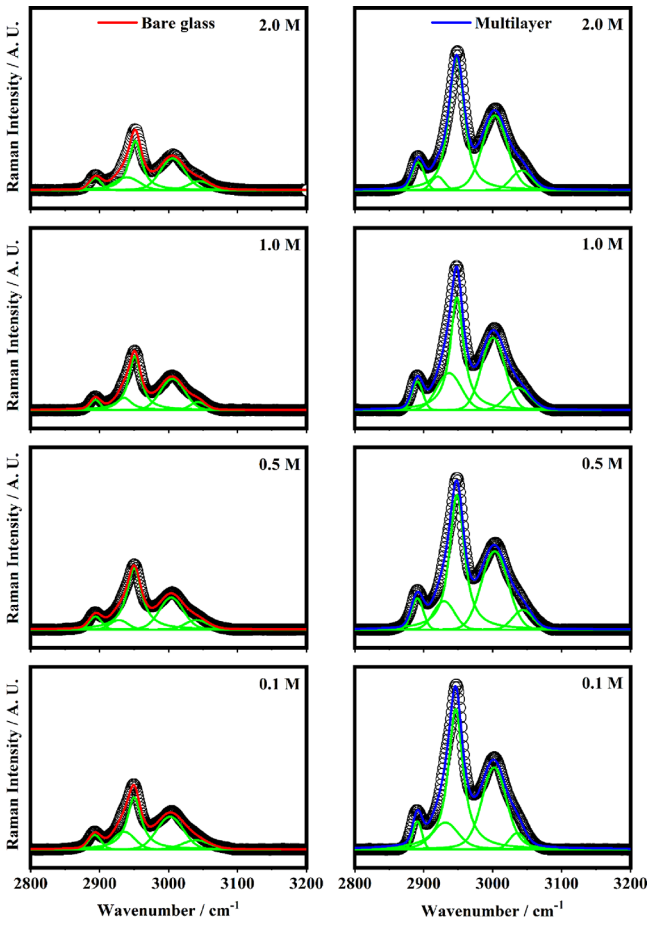

Figure 6. Fitting procedure of the Raman band in the range between 2800 and 3200 cm^{-1} collected on lithium perchlorate and propylene carbonate (Li-PC) solutions at the concentrations 0.1, 0.5, 1.0, and 2.0 M deposited on bare glass (on the left) and multilayer (on the right) substrates. The black circle represents the experimental data. The solid green lines are the Voigt curves, and the solid lines represent the total fit curves of the spectra collected on the bare glass (red) and multilayer (blue) substrates.

$$R_2 = \frac{I_{M,860} + I_{M,923} + I_{M,944} + I_{M,964}}{I_{G,860} + I_{G,923} + I_{G,944} + I_{G,964}} \quad (2)$$

$$R_3 = \frac{I_{M,1464} + I_{M,1494}}{I_{G,1464} + I_{G,1494}} \quad (3)$$

$$R_4 = \frac{I_{M,2892} + I_{M,2935} + I_{M,2950} + I_{M,3002} + I_{M,3039}}{I_{G,2892} + I_{G,2935} + I_{G,2950} + I_{G,3002} + I_{G,3039}} \quad (4)$$

where the subscripts M and G indicate the multilayer substrate and bare glass substrate, respectively, the numbers represent the Raman shift of the bands, and I represent the intensities of the relative bands.

Figure 7 highlights that, for all the concentrations, all the ratios plotted versus the concentration are more than twice, meaning that the effect of depositing the Li-PC solutions on multilayer substrates increases the intensities of the detected Raman bands.

To investigate in-depth the obtained SERS effect, Figure 8 illustrates the intensities of the Raman bands collected for the solution of Li-PC deposited on both bare glass and multilayer

https://doi.org/10.1021/acs.jpcc.3c02406
J. Phys. Chem. C 2023, 127, 12751−12759

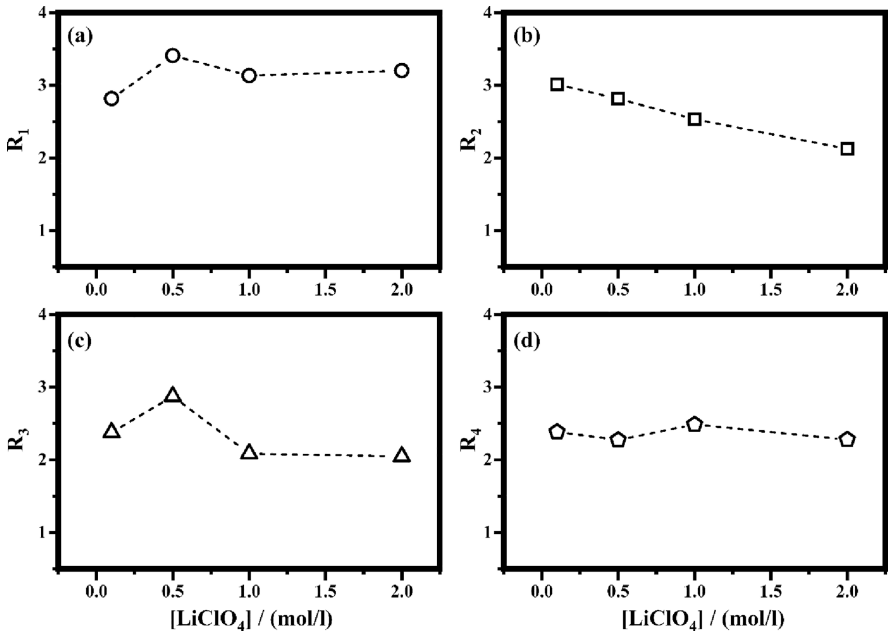

Figure 7. Trends of the intensity ratios of the bands of the Raman spectra collected on lithium perchlorate and propylene carbonate (Li-PC) solutions at the concentrations 0.1, 0.5, 1.0, and 2.0 M as described by eqs 1−4: (a) $R_1 = (I_{M,440} + I_{M,460})/(I_{G,440} + I_{G,460})$, (b) $R_2 = (I_{M,860} + I_{M,923} + I_{M,944} + I_{M,964})/(I_{G,860} + I_{G,923} + I_{G,944} + I_{G,964})$, (c) $R_3 = (I_{M,1464} + I_{M,1494})/(I_{G,1464} + I_{G,1494})$, and (d) $R_4 = (I_{M,2892} + I_{M,2935} + I_{M,2950} + I_{M,3002} + I_{M,3039})/(I_{G,2892} + I_{G,2935} + I_{G,2950} + I_{G,3002} + I_{G,3039})$.

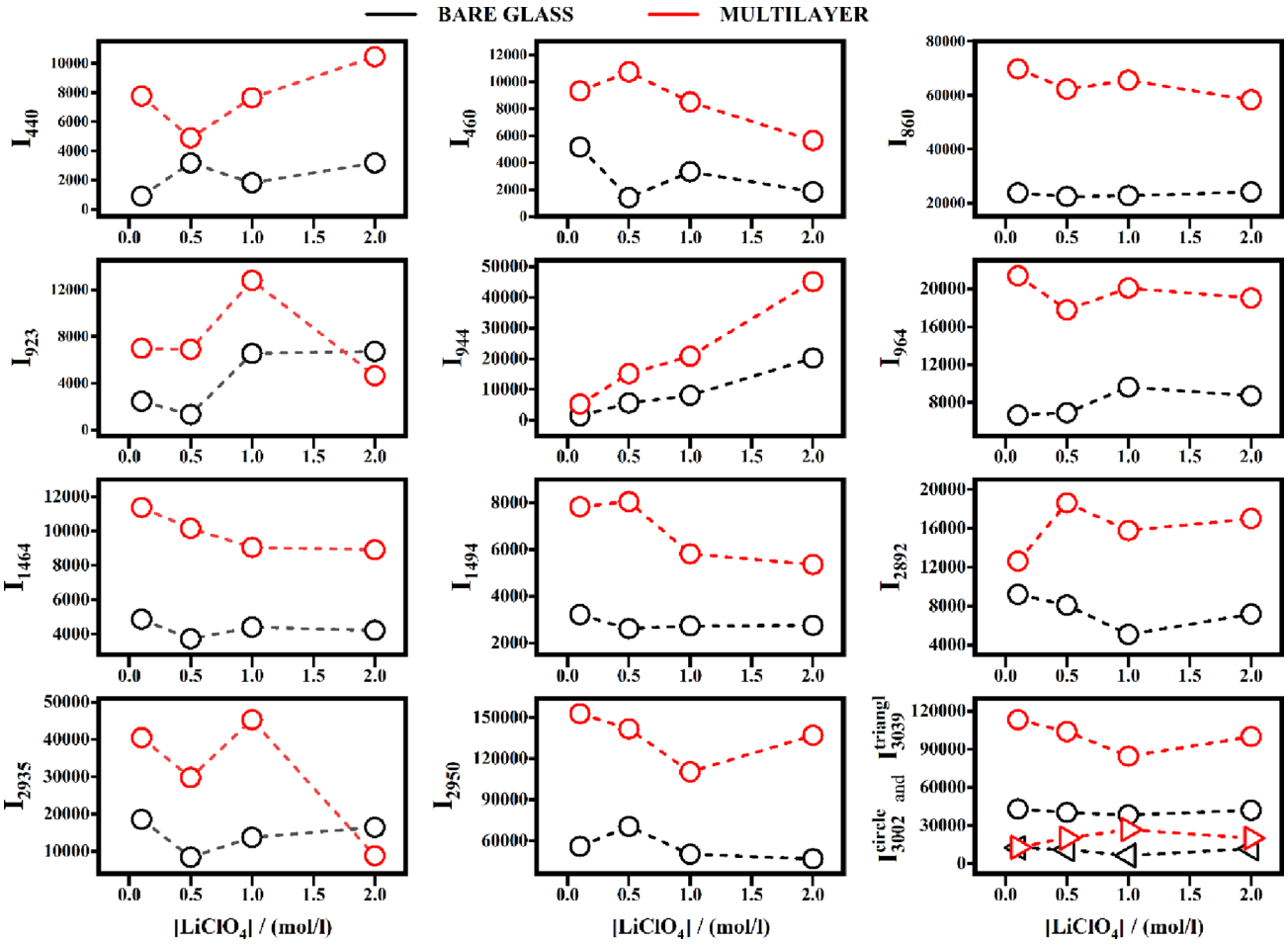

Figure 8. Trends of the intensity of the bands of the Raman spectra collected on lithium perchlorate and propylene carbonate (Li-PC) solutions at the concentrations 0.1, 0.5, 1.0, and 2.0 M deposited on the bare glass substrate (black color) and multilayer substrate (red color).

https://doi.org/10.1021/acs.jpcc.3c02406
J. Phys. Chem. C 2023, 127, 12751−12759

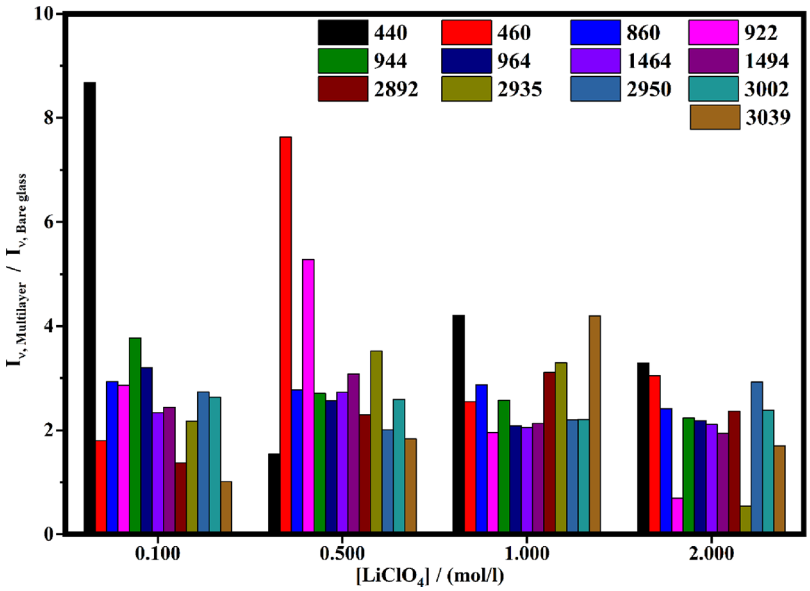

Figure 9. Intensity ratios of each band of the Raman spectra collected for lithium perchlorate and propylene carbonate (Li-PC) solutions at the concentrations 0.1, 0.5, 1.0, and 2.0 M deposited on the multilayer substrate and bare glass substrate.

substrates, highlighting that not all the bands grew with the same proportionality.

Figure 9 reports the intensity ratios of each band of the Raman spectra collected for the Li-PC solution deposited on the multilayer substrates divided by the corresponding band on the bare glass, at each concentration, which can be used as an estimation of the enhancement factor on each detected band.

As it is possible to see in Figure 9, higher enhancement factor values are obtained for the band at 440 cm^{-1} at a concentration of 0.1 mol/l and for the bands at 460 and 922 cm^{-1} for a concentration at 0.5 mol/l. However, the average values of the $I_{Multilayer}/I_{Bare\ glass}$ for all the bands are 2.9, 3.1, 2.7, and 2.1 at the following concentrations: 0.1, 0.5, 1.0, and 2.0 M, respectively. Therefore, it indicates that the effect of the enhancement is greater in solutions with lower concentrations with respect to those with higher concentrations. This can be explained by considering the fact that the higher Raman wavenumber bands belong to the solvent and, if the concentration increases, the number of solvent molecules that can be affected by the SERS effect decreases, and for this reason, the ratios shown above behave as described.

In Table 1, the values of $Abs(I_{\nu,Multilayer} - I_{\nu,Bare\ glass})$ obtained at each frequency and at each concentration are reported.

It is interesting that in this case, the difference $Abs(I_{\nu,Multilayer} - I_{\nu,Bare\ glass})$ shows values of dozens of thousands of units, meaning that their detectability improved very much when the solutions are deposited on the multilayer substrate with respect to bare glass substrates.

Table 1. Values of the Module of the Difference between the Intensity of Each Band of the Raman Spectra Collected on the Li-PC Solution Deposited on the Multilayer Substrates and the Corresponding Band Obtained from the Spectra Collected on the Solution Deposited on the Bare Glass Substrates, $Abs(I_{\nu,Multilayer} - I_{\nu,Bare\ glass})$, at Each Frequency and at Each Concentration

	[LiClO4] (mol/l)			
Raman band (cm^{-1})	0.1	0.5	1.0	2.0
440	6855	1717	5826	7272
460	4149	9319	5166	3786
860	**45985**	**39807**	**42770**	**34127**
922	4541	5576	6246	2068
944	3877	9551	12749	24913
964	14701	10862	10439	10331
1464	6506	6432	4643	4687
1494	4620	5434	3091	2601
2892	3417	10514	10685	9794
2935	**21856**	**21306**	**31530**	7602
2950	**96965**	**71319**	**60218**	**90230**
3002	**70223**	**63657**	**46202**	**58049**
3039	214	9077	20357	8281

4. CONCLUSIONS

To conclude, in this work, the possibility to enhance the SERS detection of Li-PC solutions exploiting Fano resonance produced by a metal/dielectric metamaterial as a substrate was investigated. The deconvolution procedure of the Raman bands located in the ranges from 400 to 500 cm^{-1}, 800 to 1000 cm^{-1}, 1430 to 1550 cm^{-1}, and 2800 and 3200 cm^{-1} was proposed using the Voigt profile to calculate the intensities of the bands of the Raman spectra of the Li-PC solutions deposited on the multilayer and bare glass substrates. The obtained results demonstrate that the multilayer system behaves as a SERS substrate increasing the scattering of all the Raman bands of the Li-PC solutions. The calculated average values of the enhancement, intended as the ratio $I_{\nu,Multilayer}/I_{\nu,Bare\ glass}$ for all the bands, are 2.9, 3.1, 2.7, and 2.1 at 0.1, 0.5, 1.0, and 2.0 M, respectively, indicating better performance with a lower concentration. This is confirmed also by some specific bands, e.g., 440, showing an enhancement of more than 8.

In addition, an estimation of the increase in the intensities of each band, in terms $Abs(I_{\nu,Multilayer} - I_{\nu,Bare\ glass})$, highlights a signal enhancement of more than dozens of thousands of units.

The investigated system can be thought as a proof-of-concept design for developing low-cost and large-area SERS substrates. Other studies are on the way to better understand

https://doi.org/10.1021/acs.jpcc.3c02406
J. Phys. Chem. C 2023, 127, 12751−12759

how the multilayer composition affects the enhancement of the scattered radiation and its dependency on the wavelengths.

AUTHOR INFORMATION

Corresponding Authors

Antonio Ferraro − *Consiglio Nazionale delle Ricerche - Istituto di Nanotecnologia (CNR-Nanotec), 87036 Rende, CS, Italy;* orcid.org/0000-0003-0189-6729; Email: antonio.ferraro@cnr.it

Marco Castriota − *Department of Physics, University of Calabria, 87036 Rende, CS, Italy; Consiglio Nazionale delle Ricerche - Istituto di Nanotecnologia (CNR-Nanotec), 87036 Rende, CS, Italy;* orcid.org/0000-0001-5996-0880; Email: marco.castriota@fis.unical.it

Authors

Carmen Rizzuto − *Department of Physics, University of Calabria, 87036 Rende, CS, Italy; Consiglio Nazionale delle Ricerche - Istituto di Nanotecnologia (CNR-Nanotec), 87036 Rende, CS, Italy;* orcid.org/0000-0001-5125-3567

Antonello Nucera − *Department of Physics, University of Calabria, 87036 Rende, CS, Italy*

Giuseppe Emanuele Lio − *Physics Department, University of Florence, 50019 Sesto Fiorentino, FI, Italy; European Laboratory for Non Linear Spectroscopy, LENS, 50019 Sesto Fiorentino, FI, Italy;* orcid.org/0000-0002-8925-7202

Riccardo Cristoforo Barberi − *Department of Physics, University of Calabria, 87036 Rende, CS, Italy; Consiglio Nazionale delle Ricerche - Istituto di Nanotecnologia (CNR-Nanotec), 87036 Rende, CS, Italy;* orcid.org/0000-0001-9713-1696

Complete contact information is available at: https://pubs.acs.org/10.1021/acs.jpcc.3c02406

Author Contributions

The manuscript was written through contributions of all authors. All authors have given approval to the final version of the manuscript.

Notes

The authors declare no competing financial interest.
Any additional relevant notes should be placed here.

ACKNOWLEDGMENTS

The Unical team thank the project "DEMETRA − Sviluppo di tecnologie di materiali e di tracciabilità per la sicurezza e la qualità dei cibi" PON ARS01 00401. G.E.L. thanks the research project "FSE-REACT EU" financed by National Social Fund - National Operative Research Program and Innovation 2014-2020 (DM 1062/2021).

REFERENCES

(1) Cialla, D.; März, A.; Böhme, R.; Theil, F.; Weber, K.; Schmitt, M.; Popp, J. Surface-Enhanced Raman Spectroscopy (SERS): Progress and Trends. *Anal. Bioanal. Chem.* **2012**, *403*, 27−54.

(2) Fleischmann, M.; Hendra, P. J.; McQuillan, A. J. Raman Spectra of Pyridine Adsorbed at a Silver Electrode. *Chem. Phys. Lett.* **1974**, *26*, 163−166.

(3) Sharma, B.; Frontiera, R. R.; Henry, A.-I.; Ringe, E.; Van Duyne, R. P. SERS: Materials, Applications, and the Future. *Mater. Today* **2012**, *15*, 16−25.

(4) Wang, M.; Benford, M.; Jing, N.; Coté, G.; Kameoka, J. Optofluidic Device for Ultra-Sensitive Detection of Proteins Using Surface-Enhanced Raman Spectroscopy. *Microfluid. Nanofluid.* **2009**, *6*, 411−417.

(5) Cialla, D.; Pollok, S.; Steinbrücker, C.; Weber, K.; Popp, J. SERS-Based Detection of Biomolecules. *NANO* **2014**, *3*, 383−411.

(6) Qian, C.; Guo, Q.; Xu, M.; Yuan, Y.; Yao, J. Improving the SERS Detection Sensitivity of Aromatic Molecules by a PDMS-Coated Au Nanoparticle Monolayer Film. *RSC Adv.* **2015**, *5*, 53306−53312.

(7) Mosier-Boss, P. A.; Lieberman, S. H. Detection of Volatile Organic Compounds Using Surface Enhanced Raman Spectroscopy Substrates Mounted on a Thermoelectric Cooler. *Anal. Chim. Acta* **2003**, *488*, 15−23.

(8) Cheng, F.; Xu, H.; Wang, C.; Gong, Z.; Tang, C.; Fan, M. Surface Enhanced Raman Scattering Fiber Optic Sensor as an Ion Selective Optrode: The Example of Cd 2+ Detection. *RSC Adv.* **2014**, *4*, 64683−64687.

(9) Zhang, Y.; Wang, Z.; Wu, L.; Pei, Y.; Chen, P.; Cui, Y. Rapid Simultaneous Detection of Multi-Pesticide Residues on Apple Using SERS Technique. *Analyst* **2014**, *139*, 5148−5154.

(10) Kubackova, J.; Fabriciova, G.; Miskovsky, P.; Jancura, D.; Sanchez-Cortes, S. Sensitive Surface-Enhanced Raman Spectroscopy (SERS) Detection of Organochlorine Pesticides by Alkyl Dithiol-Functionalized Metal Nanoparticles-Induced Plasmonic Hot Spots. *Anal. Chem.* **2015**, *87*, 663−669.

(11) Zhang, H.; Kang, Y.; Liu, P.; Tao, X.; Pei, J.; Li, H.; Du, Y. Determination of Pesticides by Surface-Enhanced Raman Spectroscopy on Gold-Nanoparticle-Modified Polymethacrylate. *Anal. Lett.* **2016**, *49*, 2268−2278.

(12) Candreva, A.; Di Maio, G.; Parisi, F.; Scarpelli, F.; Crispini, A.; Godbert, N.; Ricciardi, L.; Nucera, A.; Rizzuto, C.; Barberi, R. C.; Castriota, M.; La Deda, M. Luminescent Self-Assembled Monolayer on Gold Nanoparticles: Tuning of Emission According to the Surface Curvature. *Chemosensors* **2022**, *10*, 176.

(13) Caruso, T.; Castriota, M.; Policicchio, A.; Fasanella, A.; De Santo, M. P.; Ciuchi, F.; Desiderio, G.; La Rosa, S.; Rudolf, P.; Agostino, R. G.; Cazzanelli, E. Thermally Induced Evolution of Sol−Gel Grown WO3 Films on ITO/Glass Substrates. *Appl. Surf. Sci.* **2014**, *297*, 195−204.

(14) Nucera, A.; Grillo, R.; Rizzuto, C.; Barberi, R. C.; Castriota, M.; Bürgi, T.; Caputo, R.; Palermo, G. Effect of the Combination of Gold Nanoparticles and Polyelectrolyte Layers on SERS Measurements. *Biosensors* **2022**, *12*, 895.

(15) Politano, G. G.; Cazzanelli, E.; Versace, C.; Vena, C.; De Santo, M. P.; Castriota, M.; Ciuchi, F.; Bartolino, R. Graphene Oxide on Magnetron Sputtered Silver Thin Films for SERS and Metamaterial Applications. *Appl. Surf. Sci.* **2018**, *427*, 927−933.

(16) Politano, G. G.; Cazzanelli, E.; Versace, C.; Castriota, M.; Desiderio, G.; Davoli, M.; Vena, C.; Bartolino, R. Micro-Raman Investigation of Ag/Graphene Oxide/Au Sandwich Structure. *Mater. Res. Express* **2019**, *6*, No. 075605.

(17) Mosier-Boss, P. Review of SERS Substrates for Chemical Sensing. *Nanomaterials* **2017**, *7*, 142.

(18) Palermo, G.; Rippa, M.; Conti, Y.; Vestri, A.; Castagna, R.; Fusco, G.; Suffredini, E.; Zhou, J.; Zyss, J.; De Luca, A.; Petti, L. Plasmonic Metasurfaces Based on Pyramidal Nanoholes for High-Efficiency SERS Biosensing. *ACS Appl. Mater. Interfaces* **2021**, *13*, 43715−43725.

(19) Dörfer, T.; Schmitt, M.; Popp, J. Deep-UV Surface-Enhanced Raman Scattering. *J. Raman Spectrosc.* **2007**, *38*, 1379−1382.

(20) Caputo, R.; Lio, G. E. *Hybrid Flatland Metastructures*. 20210930.

(21) Caligiuri, V.; De Luca, A. Inter-Cavity Coupling Strength Control in Metal/Insulator Multilayers for Hydrogen Sensing. *Photonics* **2021**, *8*, 537.

(22) Aulika, I.; Zubkins, M.; Butikova, J.; Purans, J. Enhanced Reflectivity Change and Phase Shift of Polarized Light: Double Parameter Multilayer Sensor. *Phys. Status Solidi A* **2022**, *219*, 2100424.

(23) Lio, G. E.; Ferraro, A.; Kowerdziej, R.; Govorov, A. O.; Wang, Z.; Caputo, R. Engineering Fano-Resonant Hybrid Metastructures

with Ultra-High Sensing Performances. *Adv. Opt. Mater.* **2023**, 2203123.
(24) Lee, K.-T.; Han, S. Y.; Park, H. J. Omnidirectional Flexible Transmissive Structural Colors with High-Color-Purity and High-Efficiency Exploiting Multicavity Resonances. *Adv. Opt. Mater.* **2017**, *5*, 1700284.
(25) Lio, G. E.; Ferraro, A.; Giocondo, M.; Caputo, R.; De Luca, A. Color Gamut Behavior in Epsilon Near-Zero Nanocavities during Propagation of Gap Surface Plasmons. *Adv. Opt. Mater.* **2020**, *8*, 2000487.
(26) Ferraro, A.; Bruno, M. D. L.; Papuzzo, G.; Varchera, R.; Forestiero, A.; De Santo, M. P.; Caputo, R.; Barberi, R. C. Low Cost and Easy Validation Anticounterfeiting Plasmonic Tags Based on Thin Films of Metal and Dielectric. *Nanomaterials* **2022**, *12*, 1279.
(27) Kim, J. M.; Bak, J. M.; Lim, B.; Jung, Y. J.; Park, B. C.; Park, M. J.; Park, J. M.; Lee, H.; Jung, S.-H. Background Color Dependent Photonic Multilayer Films for Anti-Counterfeiting Labeling. *Nanoscale* **2022**, *14*, 5377−5383.
(28) Ferraro, A.; Lio, G. E.; Bruno, M. D. L.; Nocentini, S.; De Santo, M. P.; Wiersma, D. S.; Riboli, F.; Caputo, R.; Barberi, R. C. Hybrid Camouflaged Anticounterfeiting Token in a Paper Substrate. *Adv. Mater. Technol.* **2023**, *8*, 2201010.
(29) Jin, S.; Xiao, M.; Zhang, W.; Wang, B.; Zhao, C. Daytime Sub-Ambient Radiative Cooling with Vivid Structural Colors Mediated by Coupled Nanocavities. *ACS Appl. Mater. Interfaces* **2022**, *14*, 54676−54687.
(30) Ao, X.; Li, B.; Zhao, B.; Hu, M.; Ren, H.; Yang, H.; Liu, J.; Cao, J.; Feng, J.; Yang, Y.; Qi, Z.; Li, L.; Zou, C.; Pei, G. Self-Adaptive Integration of Photothermal and Radiative Cooling for Continuous Energy Harvesting from the Sun and Outer Space. *Proc. Natl. Acad. Sci.* **2022**, *119*, No. e2120557119.
(31) ElKabbash, M.; Letsou, T.; Jalil, S. A.; Hoffman, N.; Zhang, J.; Rutledge, J.; Lininger, A. R.; Fann, C.-H.; Hinczewski, M.; Strangi, G.; Guo, C. Fano-Resonant Ultrathin Film Optical Coatings. *Nat. Nanotechnol.* **2021**, *16*, 440−446.
(32) Bradley, M. *Curve Fitting in Raman and IR Spectroscopy: Basic Theory of Line Shapes and Applications*. https://www.semanticscholar.org/paper/Curve-Fitting-in-Raman-and-IR-Spectroscopy%3A-Basic-Bradley/b7af90bb8e17747eb33725b8ce9b584790fb67b8 (accessed 2022-07-20).
(33) Battisti, D.; Nazri, G. A.; Klassen, B.; Aroca, R. Vibrational Studies of Lithium Perchlorate in Propylene Carbonate Solutions. *J. Phys. Chem.* **1993**, *97*, 5826−5830.
(34) Mitterböck, M.; Fleissner, G.; Hallbrucker, A.; Mayer, E. Anomalous Contact-Ion Pairing in the Glassy States of "Dilute" Aqueous Lithium and Sodium Perchlorate Solution. *J. Phys. Chem. B* **1999**, *103*, 8016−8025.
(35) Cvjetićanin, N. D.; Šašić, S. Raman Spectroscopic Study of Lithium and Sodium Perchlorate Association in Propylene Carbonate−Water Mixed Solvents. *J. Raman Spectrosc.* **2000**, *31*, 871−876.
(36) Janz, G. J.; Ambrose, J.; Coutts, J. W.; Downey, J. R. Raman Spectrum of Propylene Carbonate. *Spectrochim. Acta, Part A* **1979**, *35*, 175−179.
(37) Schultz, Z. Demystifying SERS: A Newcomer's Guide to Using Surface Enhanced Raman Scattering. *Spectroscopy* **2020**, *35*, 15−19.

https://doi.org/10.1021/acs.jpcc.3c02406
J. Phys. Chem. C 2023, 127, 12751−12759